Impact of Oscillator Noise in Bistatic and Multistatic SAR

Gerhard Krieger, Marc Rodriguez Cassola, Marwan Younis, Robert Metzig

Microwaves and Radar Institute
German Aerospace Centre (DLR)
82234 Oberpfaffenhofen, Germany
E-Mail: Gerhard.Krieger@dlr.de

Abstract—**This paper addresses the impact of limited oscillator stability in bi- and multistatic SAR. Oscillator noise deserves special attention in distributed SAR systems, since there is no cancellation of low frequency phase errors as in a monostatic SAR, where the same oscillator signal is used for modulation and demodulation. We show that uncompensated phase noise may cause a time variant shift, spurious sidelobes, and a widening of the impulse response, as well as a low frequency phase modulation of the focused SAR signal. Quantitative estimates are derived analytically for each of these errors based on a systems theoretic model taking into account the second-order statistics of the oscillator phase noise.**

I. INTRODUCTION

Bistatic and multistatic SAR systems operate with multiple receive antennas which are mounted on different platforms [1] [2]. Such a spatial separation has several operational advantages which will increase the capability, reliability, and flexibility of future spaceborne SAR missions [3][4]. Powerful applications of bi- and multistatic satellite configurations are single-pass cross-track and along-track interferometry [5]-[8], high resolution wide swath SAR imaging [9][10], bistatic imaging for improved scene classification [11][12], resolution enhancement [13][5], SAR tomography [14][15], and frequent monitoring [16][4]. However, the implementation of bi- and multistatic SAR missions raises also a couple of new challenges like collision avoidance in close satellite formations [3][4], orbit design for the provision of appropriate baselines [5][7], increased susceptibility to ambiguities [5][10], and instrument synchronisation [19][1][17][12][18][4].

This paper addresses the impact of limited oscillator stability in bi- and multistatic SAR. Oscillator errors deserve special attention in distributed SAR systems, since there is no cancellation of low frequency phase errors as in a monostatic SAR where the same oscillator signal is used for modulation and demodulation [19]. For a quantitative investigation, we introduce in Sect. II a systems theoretic model which describes residual phase errors of ultra stable oscillators (USOs) in the framework of stochastic processes. In Sect. III, we will then show that uncompensated phase noise may cause a time variant shift, spurious sidelobes, and a widening of the bistatic impulse response, as well as a low frequency phase modulation of the focused SAR signal. The error for each contribution is derived analytically by an appropriately weighted integration of the power spectral density which models the second-order phase fluctuations of the independent USOs.

II. MODELLING OF OSCILLATOR PHASE ERRORS

A. Phase Spectrum

Random phase noise is often modelled by a second-order stationary stochastic process, which is conveniently characterised in the Fourier frequency domain by its power spectral density $S_\varphi(f)$, where $S_\varphi(f)$ describes the one-sided spectral density of phase fluctuations in units of radians squared per Hertz bandwidth at Fourier frequency f from the carrier [22][23]. Figure 1 shows a typical phase spectrum $S_\varphi(f)$ of an ultra stable oscillator (USO) with a frequency of $f_{osc} = 10$ MHz.
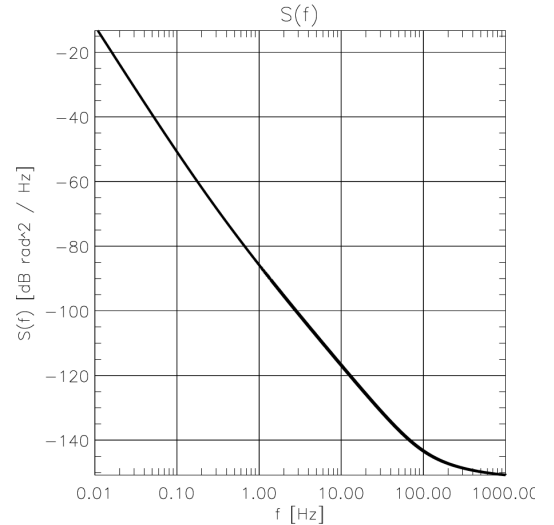

Figure 1. Power spectral density $S_\varphi(f)$ of oscillator phase noise (low frequency values correspond to a Allan standard deviation [22] with $\sigma_a(\tau=1s)\approx1*10^{-11}$, $\sigma_a(\tau=10s)\approx2*10^{-11}$, $\sigma_a(\tau=100s)\approx6*10^{-11}$).

The phase spectrum in Figure 1 can analytically be described by a linear superposition of five different frequency components [22][23]

$$S_\varphi(f) = a \cdot f^{-4} + b \cdot f^{-3} + c \cdot f^{-2} + d \cdot f^{-1} + e \qquad (1)$$

where the coefficients a to e describe the contributions from (a) random walk frequency noise, (b) frequency flicker noise, (c) white frequency noise, (d) flicker phase noise, and (e) white phase noise, respectively. The illustration in Figure 1 uses {a=-95dB, b=-90dB, c=-200.0dB, d=-130.0dB, e=-155.0dB}, which can be regarded as a representative example for the USO of current spaceborne SAR systems.

B. Phase Errors in Bistatic Radar

Simulation examples of the predicted bistatic phase errors in X-band are shown in Figure 2 for a time interval of 50 sec. Note that for better illustration the contributions from a linear phase ramp corresponding to different transmit and receive oscillator frequencies have been suppressed for each realisation of the stochastic process.
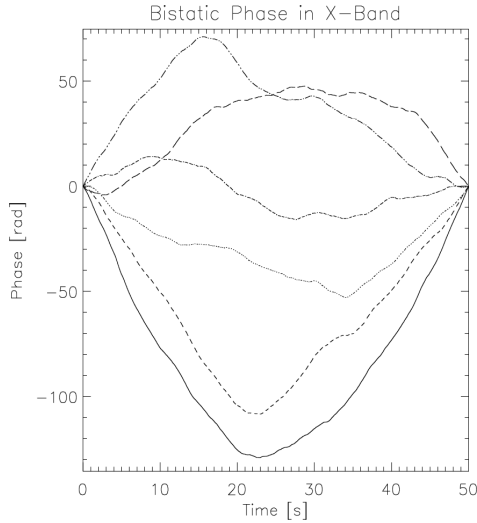

Figure 2. Example of bistatic phase errors in X-band for two independent oscillators. Shown are six realisations of the stochastic process defined by Fig. 1 after subtraction of a linear phase ramp.

C. Errors after Bistatic SAR Processing

After bistatic SAR processing, oscillator phase errors manifest themselves as a deterioration of the impulse response function (IRF). A time series of focused azimuth responses is shown in Figure 3 for a coherent integration time of $T_A = 1$ s (no weighting has been used). It becomes evident that oscillator phase noise may not only defocus the SAR image, but it may also introduce significant positioning (and phase) errors along the scene extension.
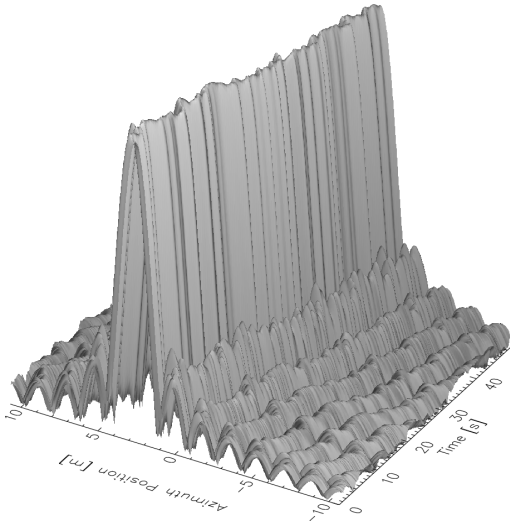

Figure 3. Focused azimuth response as a function of time ($T_A = 1$ sec, $v_{sat} = 7$ km/s, $r_0 = 800$ km, $\lambda = 3.1$cm).

III. IMPACT OF PHASE ERRORS IN BISTATIC SAR

Phase errors in both mono- and bistatic SAR may cause a time variant shift of the mainlobe, spurious sidelobes, and a widening of the impulse response, as well as phase errors in the focused SAR signal [20][21].

A. Spurious Sidelobes

High frequency phase noise will cause spurious sidelobes in the impulse response function. This deterioration can be characterised by the integrated sidelobe ratio (ISLR) which measures the transfer of signal energy from the mainlobe to the sidelobes. Note that due to the steep decay of the phase spectrum, 'high frequency' phase errors will mainly cause a transfer of the signal energy from the mainlobe to the first sidelobes (cf. simulation example in Figure 3). For an azimuth integration time T_A, the deterioration of the ISLR may be approximated from the phase spectrum as [19][1][20]:

$$\text{ISLR} \approx \sigma_\varphi^2 = 2 \cdot \left(\frac{f_0}{f_{osc}}\right)^2 \cdot \int\limits_{1/T_A}^{\infty} S_\varphi(f) \cdot df \qquad (2)$$

The factor 2 is due to the use of two independent oscillators and the scaling factor in the parentheses is due to the multiplication of the oscillator frequency f_{osc} by (f_0/f_{osc}) to obtain the radar signal with centre (carrier) frequency f_0. The upper integration limit may be substituted by the inverse of the transmit pulse duration, since higher frequency phase errors are averaged during range compression. Figure 4 shows estimates of the ISLR for the phase spectrum given in Figure 1. A typical requirement for the maximum tolerable ISLR is -20 dB which would − in this prototypical example − enable a maximum coherent integration time T_A of 2 s in X-band and 10 s in L-band, respectively. Such a prediction is also in good (qualitative) agreement with the results from several airborne bistatic radar experiments [19][24][12][25][26].
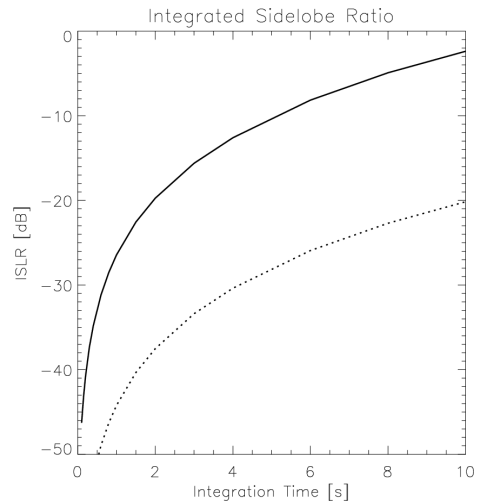

Figure 4. Integrated sidelobe ratio (ISLR) for X-band (solid) and L-band (dotted).

B. Mainlobe Dispersion

Quadratic phase errors will cause a widening of the azimuth response [20][21]. For a bistatic SAR, these errors may be approximated by

$$\sigma_Q^2 = 2 \cdot \left(\frac{f_0}{f_{osc}}\right)^2 \cdot \frac{(\pi T_A)^4}{4} \cdot \int\limits_0^{1/T_A} f^4 \cdot S_\varphi(f) \cdot df \qquad (3)$$

A typical requirement for quadratic phase errors is $\sigma_Q < \pi/2$ which would lead to a resolution loss of ca. 10 % in case of an unweighted azimuth processing [20]. Figure 5 shows estimates of the quadratic phase errors in X- and L-band for the phase spectrum $S_\varphi(f)$ of Figure 1. In this example, an integration time up to approx. 4 s would still be tolerable in X-band ensuring good bistatic focusing of the impulse response.
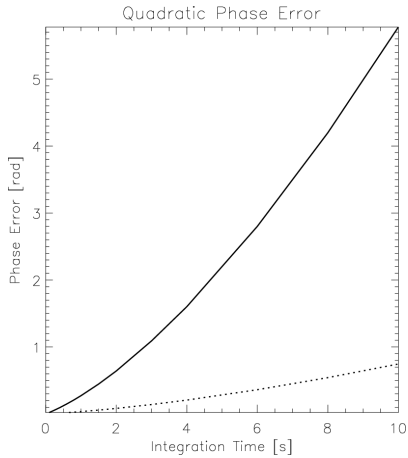

Figure 5. Quadratic phase errors for X-band (solid) and L-band (dotted).

C. Azimuth Displacement

Any difference in the oscillator frequencies of the transmitter and receiver will cause a shift of the bistatic impulse response. For a non-squinted quasi-monostatic imaging geometry, the azimuth shift is given by

$$\Delta x = \frac{c_0 r_0}{2 v_{sat}} \cdot \frac{\Delta f}{f_{osc}} \qquad (4)$$

where v_{sat} is the satellite velocity, r_0 is the slant range, and $(\Delta f/f_{osc})$ is the relative frequency deviation between the two USOs. Note that a frequency deviation of only 1 Hz between two 10 MHz oscillators (corresponding to a relative frequency deviation of 10^{-7}) will cause a constant azimuth shift of $\Delta x = 1,7$ km for $v_{sat} = 7$ km/s and $r_0 = 800$ km. This constant shift can be corrected for by ground control points or by an appropriate phase referencing system. In case of the simultaneous acquisition of both mono- and bistatic SAR data (as e.g. in the TanDEM-X mission, [8]), it is also possible to estimate such a shift by an appropriate co-registration between the monostatic and the bistatic SAR images. The variance of the remaining azimuth shift may then be derived from the spectral representation of the Allan variance with nonadjacent samples (cf. [23]) as

$$\sigma_{\Delta x}^2 = \left(\frac{c_0 r_0}{v_0}\right)^2 \cdot \int_0^\infty \frac{f^2}{f_{osc}^2} \cdot S_\varphi(f) \cdot \left(\frac{\sin(\pi T_A f)}{\pi T_A f}\right)^2 \cdot$$
$$\left[1 - \left(\frac{\sin(2\pi f t)}{2\sin(\pi f t)}\right)^2\right] \cdot df \qquad (5)$$

where we assume a time interval t elapsed from the last reference point. The solid curve in Figure 6 shows the standard deviation of the predicted azimuth shift for the phase spectrum in Figure 1 as a function of t. Note that the azimuth shift is independent of the wavelength.
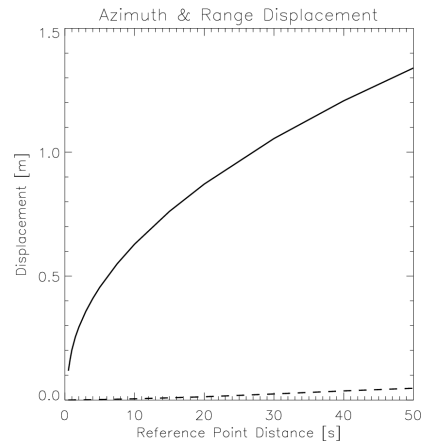

Figure 6. Azimuth (solid) and range (dashed) displacement as a function of the distance from the last reference point.

D. Range Displacement

The range shift of the impulse response will be dominated by deviations between the PRFs of the transmitter and receiver. Since the PRF is usually derived from the local oscillator by appropriate time division, the shift in slant range may be derived as

$$\Delta r(t) = \frac{c_0}{2} \cdot \left(\frac{1}{PRF_{Rx}} - \frac{1}{PRF_{Tx}}\right) \cdot t \cdot PRF_{Tx} \approx \frac{c_0}{2} \cdot \frac{\Delta f}{f_{osc}} \cdot t \qquad (6)$$

where we assumed again a quasi monostatic imaging geometry. A frequency deviation of 1 Hz between the two 10 MHz oscillators will cause a linear range drift of the impulse response by 15 m/s. From this, it becomes clear that already small frequency deviations between the local oscillators may cause rather large range shifts during one scene acquisition. This may require a periodic PRF synchronisation to adapt the receiving window to the transmit event [24], or, as an alternative, continuous recording [5]. Furthermore, very precise time referencing will be required for precise range measurements. Possible solutions for time synchronisation in a bistatic radar are discussed in [18]. An alternative is the recourse to an appropriate set of calibration targets on the ground. The residual range shift Δr may then be estimated from

$$\Delta r = \frac{\lambda}{4\pi} \cdot \Delta\varphi \qquad (7)$$

where $\Delta\varphi$ corresponds to the residual phase error not compensated by the periodic range calibration. For an estimate of $\Delta\varphi$, we assume the availability of a grid of (ground and/or phase reference) control points separated by a (temporal) distance of T_C. This will allow for the correction of low frequency phase errors up to the frequency $1/(2T_C)$. Note that in case of a linear interpolation between the control points, the remaining interferometric phase errors would be more severe as can be gauged from the estimate of quadratic phase errors in Eq. 3 and Figure 5. The variance of the residual phase error may then be approximated by

$$\sigma_\varphi^2 = 2 \cdot \left(\frac{f_0}{f_{osc}}\right)^2 \cdot \int_{1/(2T_C)}^{1/T_A} S_\varphi(f) \cdot df \qquad (8)$$

The dashed line in Figure 6 shows the expected standard deviation of the residual range shift as a function of T_C.

E.   Interferometric Phase Errors

Eq. 8 describes also the residual interferometric phase errors after a correction of low frequency phase errors up to the frequency $1/(2T_C)$. Figure 7 shows these remaining interferometric phase errors as a function of T_C. It becomes clear, that the phase error will rapidly increase with increasing control point separation T_C. This causes a low frequency modulation of the interferometric phase which affects mainly the absolute height error in case of DEM generation.
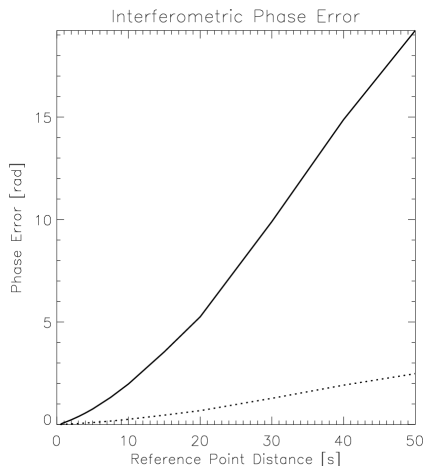

Figure 7.   Interferometric phase error for X-band (solid) and L-band (dotted).

IV.   DISCUSSION

This paper has analyzed the impact of oscillator phase noise in bi- and multistatic SAR. Based on a second-order stochastic model, quantitative estimates have been derived for potential errors like a distortion of the bistatic SAR impulse response, azimuth and range displacements, as well as interferometric phase errors. The most demanding requirements arise from multistatic interferometry. For example, the generation of high resolution digital elevation models (DEMs) will require precise relative phase knowledge in the order of a few degrees to avoid a low frequency modulation of the DEM in azimuth. Such errors require an appropriate phase referencing between the independent USOs. As can be seen from Figure 7, the required update frequency of an X-band interferometer is in the order of 1-10 Hz for the oscillator characterized in Figure 1. This requirement is reduced for longer wavelengths. Possible solutions for phase referencing are a direct exchange of radar pulses [8] or a ping-pong interferometric mode [6] in case of fully-active systems, and an appropriate bidirectional phase synchronization link in case of semi-active constellations [17]. An alternative is the use of oscillators with a significantly better long-term frequency stability in combination with a sparse net of ground control points. For example, the space qualified 5 MHz oscillators in [29] have a short term stability of $\sigma_a(\tau=10s) = 10^{-13}$ which would decrease the interferometric phase errors in Figure 7 by two orders of magnitude. Further calibration techniques will be discussed in [30].

V.   ACKNOWLEDGMENT

The author greatly appreciates the helpful discussions with S. Buckreuss on the impact of motion errors in monostatic airborne SAR.

VI.   REFERENCES

[1]   N. Willis, Bistatic Radar, Artech House, Boston, 1991.

[2]   P. Hartl and H.M. Braun, Bistatic Radar in Space, in Space Based Radar Handbook, Artech House, 1989.

[3]   M. Martin, P. Klupar, S. Kilberg, J. Winter, Techsat 21 and Revolutionizing Space Missions using Microsatellites, 15th American Institute of Aeronautics and Astronautics Conference on Small Satellites 2001, Utah, USA.

[4]   G. Krieger, A. Moreira, Spaceborne Bi- and Multistatic SAR: Potentials and Challenges, to appear in IEE Proc. Radar, Sonar, Navigation, 2005.

[5]   D. Massonnet, Capabilities and Limitations of the Interferometric Cartwheel, IEEE Trans. Geosci. Remote Sensing 39(3), pp. 506-520, 2001.

[6]   Evans, N.B., Lee, P., Girard, R., The RADARSAT-2/3 Topographic Mission, EUSAR 2002, pp. 37-39, Cologne, Germany.

[7]   G. Krieger, H. Fiedler, J. Mittermayer, K. Papathanassiou, A. Moreira, Analysis of Multi-Static Configurations for Spaceborne SAR Interfero-metry, IEE Proc. Radar, Sonar, and Navigation 150(3), pp. 87-96, 2003.

[8]   A. Moreira, G. Krieger, I. Hajnsek, M. Werner, D. Hounam, S. Riegger, E. Settelmeyer, TanDEM-X: A TerraSAR-X Add-On Satellite for Single-Pass SAR Interferometry, IGARSS 2004, Anchorage, USA.

[9]   N.A. Goodman, S.C. Lin, D. Rajakrishna, J.M. Stiles, Processing of Multiple-Receiver Spaceborne Arrays for Wide-Area SAR, IEEE Trans. Geoscience Remote Sensing, Vol. 40, No.4, 2002.

[10]   G. Krieger, N. Gebert, A. Moreira, Unambiguous SAR Signal Reconstruction for Non-Uniform Displaced Phase Centre Sampling, IEEE Geosc. and Remote Sensing Letters, Vol. 1, No. 4, pp. 260-265, 2004.

[11]   A. Moccia, G. Rufino, M. D'Errico et al. BISSAT: A Bistatic SAR for Earth Observation, ASI Research Contract I/R/213/00, Phase A Study – Final Report, 2001.

[12]   P. Dubois-Fernandez, H. Cantalloube, B. Vaizan, G. Krieger, R. Horn, M. Wendler, and V. Giroux, ONERA-DLR Bistatic SAR Campaign: Planning, Data Acquisition, and First Analysis of Bistatic Scattering Behavior of Natural and Urban Targets. To appear in IEE Proc. Radar, Sonar, Navigation, 2005.

[13]   C. Prati, F. Rocca, Improving Slant Range Resolution with Multiple SAR Surveys, IEEE Trans. Aerospace Elect. Syst., Vol. 29, No. 1, 1993.

[14]   A. Reigber, A. Moreira, First Demonstration of Airborne SAR Tomography using Multibaseline L-Band Data, IEEE Trans. Geosci. Remote Sensing, Vol. 38, pp. 2142-2152, 2000.

[15]   F. Lombardini, Differential Tomography: A New Framework for SAR Interferometry, IEEE Trans. Geosci. Remote Sens., Vol. 43, No. 1, 2005.

[16]   C. Prati, F. Rocca, D. Giancola, A.M. Guarnieri, Passive Geosynchronous SAR System Reusing Backscattered Digital Audio Broadcasting Signals, IEEE Trans. Geosci. Remote Sens.,Vol. 36, No. 6, 1998.

[17]   M. Eineder, Oscillator Clock Drift Compensation in Bistatic Interferometric SAR, Proceedings of IGARSS 2003.

[18]   M. Weiß, Time and Frequency Synchronisation Aspects for Bistatic SAR Systems, Proc. EUSAR 2004, pp. 395-398, 2004.

[19]   J.L. Auterman, Phase Stability Requirements for a Bistatic SAR, Proc. IEEE Nat. Radar Conf. 1984, pp. 48-52, Atlanta, USA.

[20]   S. Buckreuss, Bewegungskompensation für flugzeuggetragene SAR Systeme, DLR Forschungsbericht 94-17, 1994 (see also: S. Buckreuss, Motion Errors in an Airborne Synthetic Aperture Radar System, ETT-Journal, Vol. 2 , No. 6, pp. 55-64, 1991)

[21]   D. Hounam, E. Panula-Otto, K. Wägel, Oscillator Noise and SAR Image Quality, DLR Forschungsbericht, 1994.

[22]   J. Rutman, Characterization of Phase and Frequency Instabilities in Precision Frequency Sources: Fifteen Years of Progress, Proc. IEEE, Vol. 66, No. 9, pp. 1048-1073, 1978.

[23]   J.A. Barnes, A.R. Chi, L.S. Cutler et al., Characterization of Frequency Stability, IEEE Trans. Instrumentation and Measurement, Vol. 20, No. 2, pp. 105-120, 1971.

[24]   M. Wendler, G. Krieger, R. Horn et al., Results of a Bistatic Airborne SAR Experiment, Proc. International Radar Symposium 2003, DGON, pp. 247-253, Dresden, Germany.

[25]   G. Yates, A.M. Horne, A.P. Blake, R. Middleton, D.B. Andre, Bistatic SAR Image Formation, Proc. EUSAR 2004, pp. 581-584, Ulm, Germany.

[26]   J. Ender, I. Walterscheid, A. Brenner, New Aspects of Bistatic SAR: Processing and Experiments, In Proc. IGARSS 2004, Anchorage, USA.

[27]   M. Rodriguez-Cassola, G. Krieger, M. Wendler, H. Cantalloube, P. Dubois Fernandez, Azimuth-invariant, Bistatic Airborne SAR Processing Strategies Based on Monostatic Algorithms, IGARSS 2005.

[28]   G. Krieger, H. Fiedler, M. Eineder, M. Werner, A. Moreira, TanDEM-X: Mission Concept and Performance Analysis, IGARSS 2005.

[29]   V. Candelier, P. Canzian, J. Lamboley, M. Brunet, G. Santarelli, Space Qualified 5 MHz Ultra Stable Oscillators, Intern. Frequency Control Symp. 2003, pp. 575–582, Tampa, Fl., USA.

[30]   G. Krieger, A. Moreira, Multistatic SAR Satellite Configurations: Potentials and Challenges, IGARSS 2005, Seoul, Korea.